# ANNUAL REVIEWS

*Annual Review of Fluid Mechanics*

# Chemo-Hydrodynamic Patterns and Instabilities

## A. De Wit

Nonlinear Physical Chemistry Unit, Université Libre de Bruxelles, 1050 Brussels, Belgium;
email: adewit@ulb.ac.be

## ANNUAL REVIEWS CONNECT

www.annualreviews.org

- Download figures
- Navigate cited references
- Keyword search
- Explore related articles
- Share via email or social media

## Keywords

reactive flows, viscous fingering, buoyancy-driven instabilities, Rayleigh–Taylor, double diffusion, chemical fronts, chemo-hydrodynamics

## Abstract

By modifying a physical property of a solution like its density or viscosity, chemical reactions can modify and even trigger convective flows. These flows in turn affect the spatiotemporal distribution of the chemical species. A nontrivial coupling between reactions and flows then occurs. We present simple model systems of this chemo-hydrodynamic coupling. In particular, we illustrate the possibility of chemical reactions controlling or triggering viscous fingering, Rayleigh–Taylor, double-diffusive, and convective dissolution instabilities. We discuss laboratory experiments performed to study these phenomena and compare the experimental results to theoretical predictions. In each case we contrast the chemo-hydrodynamic patterns and instabilities with those that develop in nonreactive systems and unify the different dynamics in terms of the common features of the related spatial mobility profiles.

# 1. INTRODUCTION

Hydrodynamic instabilities of miscible interfaces are encountered in many applications where two fluids are put into contact. They typically develop when gradients of a physical property are present across the interface. As an example, a Rayleigh–Taylor (RT) instability can deform the miscible contact zone into alternating rising and sinking fingers when a denser solution is put on top of a less dense one in the gravity field (see **Figure 1a**). Similarly, a viscous fingering (VF) instability can develop when a less viscous fluid displaces a more viscous one in a porous medium. Such instabilities have been thoroughly studied both experimentally and theoretically and are presently well understood. If, in contrast, the solutions contain chemicals that react such that the reaction changes the density or viscosity in situ, an interplay between reactions and hydrodynamics can occur (De Wit et al. 2012, De Wit 2016). As an example, **Figure 1** shows experimental evidence of changes in the symmetry of buoyancy-driven hydrodynamic instabilities when a reaction actively changes the density in situ. In this review, we describe the major influence that reactions can have on such instabilities. In particular, we explain how, by changing the physical property controlling the hydrodynamic flow, one can use reactions to control the location and amplitude of convective
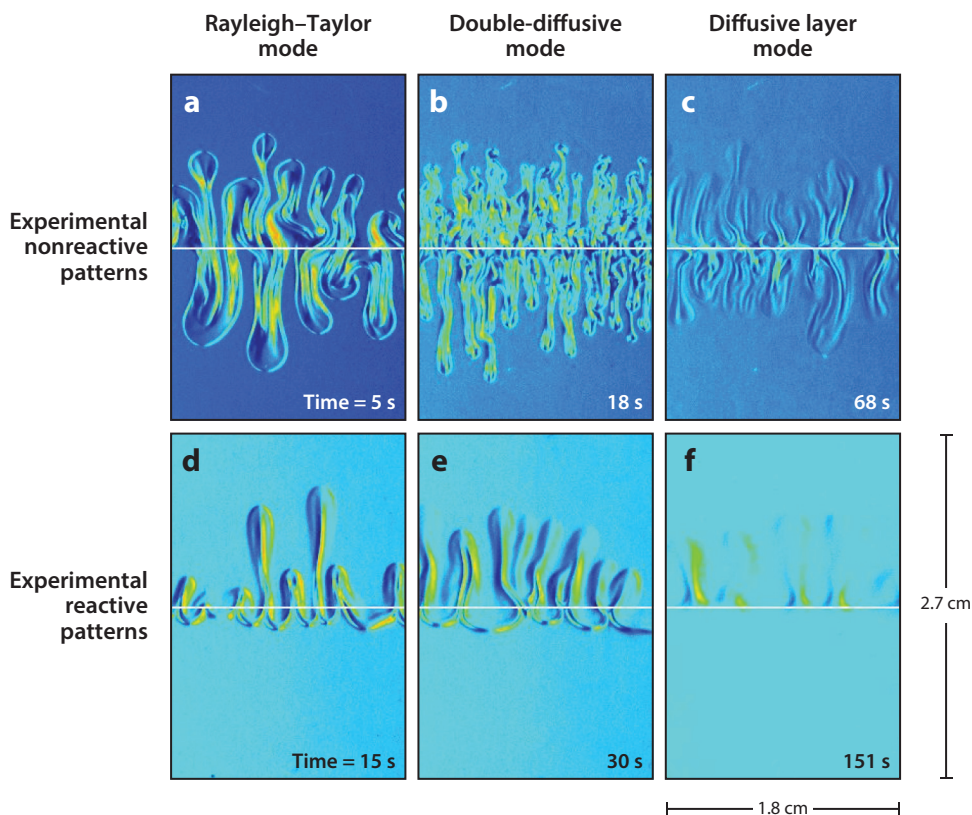


|  | Rayleigh–Taylor mode | Double-diffusive mode | Diffusive layer mode |
|---|---|---|---|

**Figure 1**

Comparison between experimental nonreactive (*a–c*) and reactive (*d–f*) buoyancy-driven patterns in a vertical Hele–Shaw cell due to (*a,d*) Rayleigh–Taylor, (*b,e*) double-diffusive, and (*c,f*) diffusive layer convection modes. The images feature gradients of index of refraction measured by an optical Schlieren method from blue (minimum value) to red (largest value). Figure adapted with permission from Lemaigre et al. (2013).

motions. As a corollary, flows can also be used to tune the yield and spatiotemporal distribution of the chemical species. This control over pattern formation in reactive fluids forms the basis of chemo-hydrodynamic pattern selection at the heart of this review.

Of course, this subject is very vast and flows of reactive fluids are encountered in numerous applications, ranging from convective motions in stars or planet interiors to atmospheric chemistry, engineering applications like combustion, blooming of bacteria in oceanic currents, and many more. We do not address here dynamics where the chemical species are passively advected (Villermaux 2019), focusing instead on reactions actively modifying or controlling convection. Moreover, dictated by the author's own research in the field, this review focuses mainly on reactive interfaces in miscible porous media flows but points out as much as possible the generality of the chemo-hydrodynamic control described. Partially miscible systems are treated only in the important case of $CO_2$ sequestration. We first introduce the mobility profile that is at the heart of the viscously and buoyancy-driven instabilities we discuss, as well as the influence of chemical reactions on them. Next, we briefly describe the properties of the hydrodynamic VF, RT, and double-diffusive (DD) instabilities in the absence of any reaction. We proceed by analyzing the effect of reactions on these hydrodynamic instabilities.

## 2. REACTIVE INTERFACE IN A POROUS MEDIUM

Consider an interface between two semi-infinite regions in a homogeneous porous medium with permeability $\kappa$. In this system, a solution of reactant $A$ with initial concentration $a_o$ is put into contact along a contact zone at initial time with a solution of another reactant $B$ with initial concentration $b_o$. The two solutions are both considered to be dilute and have their own viscosity $\mu$ and density $\rho$. In the absence of any flow, the two reactants meet by diffusion and a simple chemical reaction,

$$A + B \rightarrow C, \qquad\qquad 1.$$

takes place in the mixing zone, generating the product, $C$. We seek to understand how this reactive two-layer stratification can be destabilized by viscosity or density gradients and how the reaction can modify the properties of the hydrodynamic instability. For incompressible flows, the dynamics of miscible interfaces in porous media can be described by the following system of reaction–diffusion–convection (RDC) equations,

$$\nabla.\mathbf{u} = 0, \qquad\qquad 2.$$

$$\nabla p = -\frac{\mu}{\kappa}\mathbf{u} + \rho\mathbf{g}, \qquad\qquad 3.$$

$$\frac{\partial a}{\partial t} + \mathbf{u}.\nabla a = D_A\nabla^2 a - kab, \qquad\qquad 4.$$

$$\frac{\partial b}{\partial t} + \mathbf{u}.\nabla b = D_B\nabla^2 b - kab, \qquad\qquad 5.$$

$$\frac{\partial c}{\partial t} + \mathbf{u}.\nabla c = D_C\nabla^2 c + kab, \qquad\qquad 6.$$

where $a$, $b$, and $c$ denote respectively the concentrations of $A$, $B$, and $C$; $k$ is the kinetic constant; $p$ is the pressure; $\mathbf{u}$ is the velocity field; $\mathbf{g}$ is the gravitational acceleration; and $D_A$, $D_B$, and $D_C$ are the diffusion coefficients of the species $A$, $B$, and $C$, respectively. Equation 3 is Darcy's law relating the velocity field $\mathbf{u}$ to the gradient of pressure. The interplay between reactions and hydrodynamics

arises thanks to the dependence of either viscosity $\mu$, density $\rho$, or permeability $\kappa$ on the concentrations. Therefore, in addition to given initial and boundary conditions for all variables, the model Equations 2–6 need to be complemented in each case by a state equation expressing this dependence. This state equation will depend on the instability considered, but common features can be sketched in terms of the relevant mobility profile.

## 3. MOBILITY PROFILE

The essence of the chemical control of convective motions lies in the control of the mobility profile at the root of the hydrodynamic instability. The mobility profile $M(x)$ is here defined as the function describing the way the physical property $M$, which is the motor of the hydrodynamic instability, varies along a given spatial coordinate, $x$ (Homsy 1987, Manickam & Homsy 1995). The mobility profile is a direct consequence of the state equation. In the cases to be analyzed here, $M$ is typically the viscosity $\mu$, the density $\rho$, or the permeability $\kappa$. **Figure 2** shows various profiles $M(x)$ that can develop in miscible systems when two different fluids or two solutions of the same solvent but different chemical compositions are put into contact. As the fluids usually have different densities or viscosities, there is a jump in $M$ across the initial contact zone. Upon diffusive mixing, $M$ typically expands as an error function. **Figure 2a,b** shows two examples of such profiles at a given time after contact. Depending on the arbitrary choice of orientation of the $x$ axis, $M$ is then either decreasing (**Figure 2a**) or increasing (**Figure 2b**) along $x$. As is shown below, reactions or the presence of chemical species with different diffusion coefficients typically modify these reference mobility profiles, either by changing the gradient of $M$ or by introducing extrema in $M$ (**Figure 2c–f**). Below we review how reactions can induce these changes in the mobility profile, as well as the consequences on the dynamics. Before doing so, let us first review the hydrodynamic instabilities that can develop in the presence of monotonic mobility profiles like those of **Figure 2a,b**.
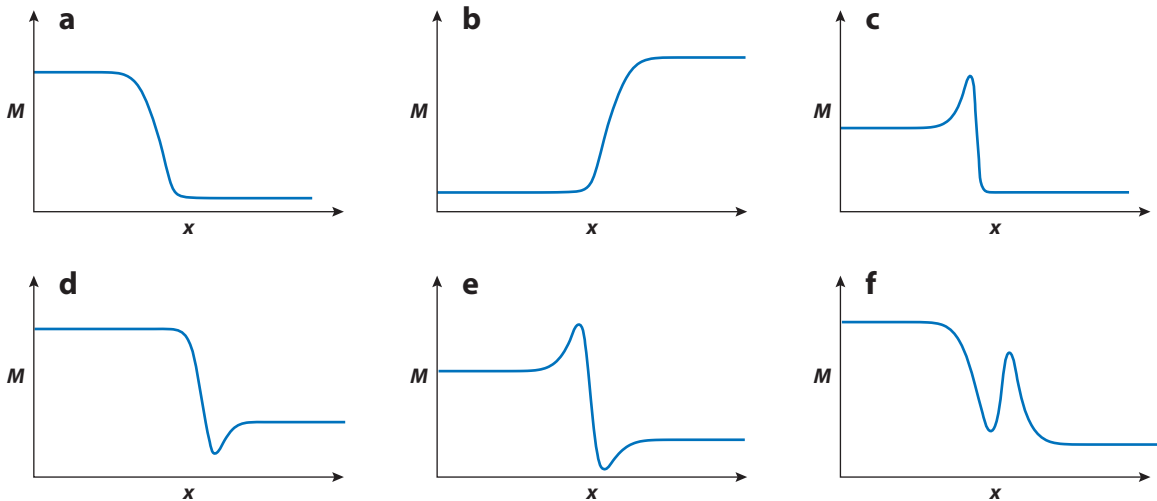


**Figure 2**

Mobility profiles $M(x)$ giving the spatial dependence of a given physical property of the fluid like its viscosity or density as a function of space. (*a*) Monotonic decreasing along $x$, (*b*) monotonic increasing along $x$, (*c*) nonmonotonic with a maximum, (*d*) nonmonotonic with a minimum, (*e*) nonmonotonic with two extrema with an amplitude outside the two end-point values of $M$, (*f*) nonmonotonic with two extrema with an amplitude inside the two end-point values of $M$.

# 4. HYDRODYNAMIC INSTABILITIES

## 4.1. Viscous Fingering

When a less viscous fluid displaces a more viscous one in a porous medium, the interface between the two is unstable to VF, inducing a fingered deformation of the miscible mixing zone (Hill 1952, Homsy 1987). In that case, the typical unstable mobility profile is the one of viscosity, such as in **Figure 2b**, where the mobility $M$ is the dynamic viscosity $\mu$ and $x$ is the direction of injection. In contrast, the reverse monotonic decreasing viscosity profile corresponding to a more viscous fluid displacing a less viscous one along $x$ (as in **Figure 2a**) is stable.

## 4.2. Buoyancy-Driven Instabilities

When density variations determine the mobility profile $M$, various instabilities can develop depending on the orientation of the interface between the two fluids $A$ and $B$ with respect to the gravity field and on the diffusivities of the species involved. To connect to reactive solutions later, let us consider a solution of species $A$ that is initially put into contact along a line with a miscible solution of $B$. Both species contribute to change the density of the solution. If the interface between the two miscible solutions is initially vertical, the mobility profiles with $M = \rho$ are those of **Figure 2a,b**, with $x$ pointing perpendicularly to the gravity field. The stratification always leads to convection as the denser solution sinks below the other one, inducing a gravity current (Meiburg & Kneller 2010).

An RT instability develops across an initially horizontal interface when a denser fluid lies above a less dense fluid in a gravity field. If $x$ points downward along the gravity field, then the unstable density profile in the nonreactive case is the one of **Figure 2a** with $M = \rho$. Regular fingers then develop symmetrically across the interface (Wooding 1969, Fernandez et al. 2002), as in **Figure 1a**. However, even when a less dense fluid is stratified on top of a denser fluid, i.e., for a density profile increasing along the direction of gravity (as in **Figure 2b**), an instability can develop due to double diffusion (Turner 1979, Radko 2013). If the lower solute $B$ diffuses faster than the upper solute $A$, then a DD instability destabilizes the interface into density fingering similar to the RT modes (see **Figure 1b**), while if $A$ diffuses faster than $B$, a diffusive layer convection (DLC) mode occurs, giving disconnected localized convective zones both above and below the interface (see **Figure 1c**) (Trevelyan et al. 2011, Carballido-Landeira et al. 2013). In miscible solutions containing two solutes $A$ and $B$ with different diffusivities, the RT and DD modes can interact, giving rise for instance to specific mixed-mode fingers, where the difference in diffusion of the species deforms the tip of the RT fingers into antennas (Carballido-Landeira et al. 2013). Similarly, DD effects can control the onset times and intensity of the convective velocity of RT modes (Gopalakrishnan et al. 2018). All of these effects are at play in reactive systems where different solutes with different diffusion coefficients are involved.

To appreciate the effect of simple bimolecular reactions on these hydrodynamic instabilities, one first needs to understand the properties of reaction–diffusion (RD) fronts, as their concentration profiles control the mobility profile at the heart of the hydrodynamics.

# 5. REACTION–DIFFUSION $A + B \rightarrow C$ CHEMICAL FRONTS

Since the pioneering work of Gálfi & Rácz (1988), researchers have thoroughly studied the properties of $A + B \rightarrow C$ RD chemical fronts, in which the reactant solutions of $A$ and $B$ in respective concentrations $a_o$ and $b_o$ are put into contact at a given position $x = 0$ at $t = 0$ and react according to a bimolecular $A + B \rightarrow C$ kinetics. When $A$ and $B$ meet by diffusion, they react, producing $C$ in
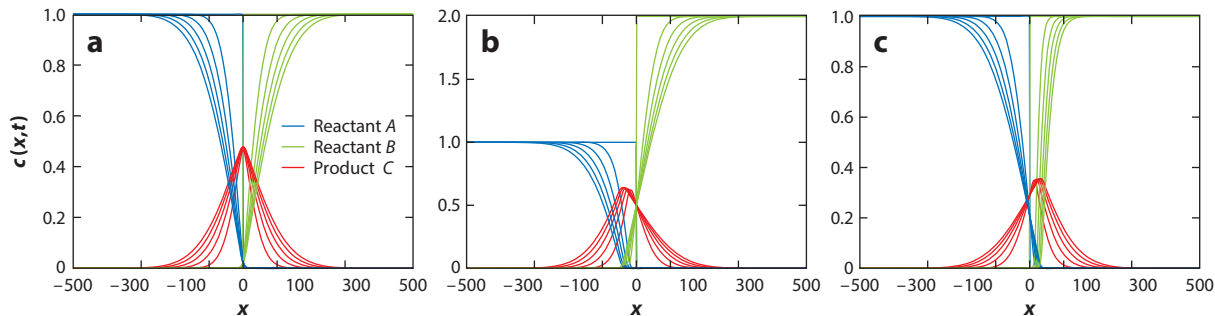
**Figure 3**

One-dimensional $A + B \rightarrow C$ reaction–diffusion dimensionless concentration profiles, shown at successive times, of reactants $A$ (*blue*) and $B$ (*green*) and product $C$ (*red*) for (*a*) equal diffusion coefficients and initial concentrations for $A$ and $B$, (*b*) equal diffusion coefficients for $A$ and $B$ but a larger concentration of $B$, and (*c*) the same initial concentrations for $A$ and $B$ but where $A$ diffuses five times faster than $B$. The position of the front at $t = 0$ is $x = 0$.

the miscible contact zone. **Figure 3** shows such RD fronts, solutions of Equations 4–6 in dimensionless form when $\mathbf{u} = 0$. Depending on the relative value of the diffusion coefficients $D_A$ and $D_B$ and on the ratio $\beta = b_o/a_o$ of their initial concentrations, the front can move in either direction. The reaction front position, defined as the location where the reaction rate is maximum, stays at $x = 0$ if $A$ and $B$ have the same diffusion coefficient and $\beta = 1$, as shown in **Figure 3a**. This is related to the fact that the diffusive flux of $A$ toward the reaction front is then the same as the flux of $B$. However, if $a_0^2 D_A$ and $b_0^2 D_B$ are not equal, these two fluxes differ and the front moves toward the region with the smallest diffusive flux (Gálfi & Rácz 1988, Jiang & Ebner 1990, Gérard & De Wit 2009). As an example, for equal diffusion coefficients, the more concentrated solution invades the other one (**Figure 3b**). On the other hand, for $\beta = 1$, the front invades the reactant of lowest diffusion coefficient (**Figure 3c**). Thus, we see that, depending on the initial concentrations and properties (and, more specifically, the diffusion coefficient) of the reactants, the RD concentration profiles of reactants $A$ and $B$ and of the product $C$ can evolve symmetrically (**Figure 3a**) with regard to the initial position of the front or can develop asymmetries (**Figure 3b,c**). This in turn affects the resulting mobility profiles if the chemical species have an active effect on density or viscosity. Let us now review what happens if the chemical species actively change the flow, starting with the effect on viscosity before addressing changes in density.

## 6. HYDRODYNAMIC INSTABILITIES IN REACTIVE FLUIDS

### 6.1. Viscous Fingering in Reactive Systems

In the absence of any reaction, VF develops when a less viscous fluid displaces a more viscous one in a porous medium. This instability has been thoroughly studied both experimentally and theoretically because of, among other reasons, its ubiquity in oil recovery when a fluid such as water displaces more viscous oil in soil (Saffman & Taylor 1958, Homsy 1987). In this context, reactions producing, for instance, surfactants in situ can modify the local surface tension and affect the Saffman–Taylor instability between two immiscible fluids (Nasr-El-Din et al. 1990, Hornof & Baig 1995, Jahoda & Hornof 2000, Fernandez & Homsy 2003, Niroobakhsh et al. 2017, Tsuzuki et al. 2019). We do not review this particular case here, as we focus on miscible systems. VF is also observed in chromatography, a separation technique by which a mixture of chemical components dissolved in a given solvent is separated via velocity-dependent dispersion at different speeds in

a porous matrix or selective adsorption on the solid phase (Guiochon et al. 2006). If the carrier fluid has a different viscosity than the sample solvent, VF can appear, which is dramatic for the efficiency of separation (Dickson et al. 1997; Broyles et al. 1998; De Wit et al. 2005; Rousseaux et al. 2007, 2011). In this context, it has been shown that adsorption on the porous matrix of components controlling the viscosity of the fluids can influence the instability (Mishra et al. 2007; Rana et al. 2014, 2018). As an example, the onset time of the instability can, in some cases, depend nonmonotonically on the retention parameter of the solute adsorption (Hota et al. 2015).

Several works have analyzed VF of miscible autocatalytic fronts that can form a self-organized interface between the reactants and products of an autocatalytic front (De Wit & Homsy 1999a, 1999b; Swernath & Pushpavanam 2007, 2008; Ghesmat & Azaiez 2009). The reactions can modify the relative stability of the front and induce the formation of isolated droplets if the reaction is bistable, i.e., admits two different stable states.

The interplay of chemistry and VF occurs through the influence of reactions on viscosity. In porous media, changes in the permeability $\kappa$ via dissolution or precipitation reactions affecting the pore space of the porous matrix can also trigger fingering. This has long been known in studies on infiltration instabilities, where the invading fluid reacts with the solid matrix, leading to a dissolution of the solid phase and an increase in porosity (Chadam et al. 1986, Daccord & Lenormand 1987, Szymczak & Ladd 2014). More recently, researchers have shown that precipitation locally decreasing the permeability can also induce fingering (Nagatsu et al. 2014), leading to beautiful precipitation patterns in various contexts, including chemical gardens (Haudin et al. 2014) or $CO_2$ mineralization reactions (White & Ward 2012, Schuszter et al. 2014). Unsurprisingly, concomitant changes in viscosity and permeability can induce an interplay between VF and precipitation-driven fingering, giving rise to interesting new patterns (Nagatsu et al. 2008a, Haudin & De Wit 2015).

## 6.2. Viscous Fingering of $A + B \rightarrow C$ Chemical Fronts

Here we explain in more detail the analytical and numerical developments that show how simple $A + B \rightarrow C$ reactions can influence or even trigger VF before explaining how these theoretical predictions allow one to understand various experimental observations.

### 6.2.1. Viscosity profiles in reactive systems.
If all three species $A$, $B$, and $C$ influence the viscosity, we have in the most general case a state equation $\mu(\mathbf{r}, t) = \mu(a, b, c)$, i.e., the viscosity profile depends on the concentration profiles $a(\mathbf{r}, t)$, $b(\mathbf{r}, t)$, and $c(\mathbf{r}, t)$ of both reactants $A$ and $B$ and the product $C$, where $\mathbf{r} = (x, y, z)$ is the position vector. This state equation couples the RDC Equations 4–6 for the concentrations to the flow Equation 3. The viscosities $\mu_A = \mu(a_0, 0, 0)$, $\mu_B = \mu(0, a_0, 0)$, and $\mu_C = \mu(0, 0, a_0)$ represent the viscosity of the fluid when only one of the chemical species is present in concentration $a_0$. For simplicity, theoretical studies usually assume an exponential relation

$$\mu = \mu_A \, e^{(R_b b + R_c c)/a_0}, \qquad\qquad 7.$$

which allows one to study Equation 3 in a simple form in the streamfunction formalism (Gérard & De Wit 2009). The problem then depends only on two parameters, $R_b$ and $R_c$, which are the log mobility ratios, defined as

$$R_b = \ln\left[\frac{\mu_B}{\mu_A}\right] \quad \text{and} \quad R_c = \ln\left[\frac{\mu_C}{\mu_A}\right]. \qquad\qquad 8.$$

The parameter $R_b$ compares the viscosity of the two reactant solutions, while $R_c$ measures the ratio between the viscosities of the product $C$ and reactant $A$ solutions. In the absence of any reaction and if $A$ is injected into $B$, VF takes place for $R_b > 0$, i.e., if the displacing solution $A$ is less viscous than the displaced solution $B$.

In the reactive case, as soon as the reactants $A$ and $B$ come into contact via diffusion, the chemical reaction is triggered, generating the product $C$ in the reactive zone (Hejazi et al. 2010). The changes in the concentrations profiles reshape the viscosity profiles, which, depending on the relative values of $R_b$ and $R_c$, can become nonmonotonic with a maximum if $C$ is sufficiently more viscous than the reactants or with a minimum if, on the contrary, $C$ is decreasing the viscosity. **Figure 4** shows such viscosity profiles in the $(R_b, R_c)$ parameter space obtained by using Equation 7 and the RD concentration profiles of **Figure 3a**.

**6.2.2. Theoretical studies.** Linear stability analysis (LSA) of these viscosity profiles modified by reactions has treated two cases depending on whether the reference nonreactive situation is unstable or stable. If the underlying nonreactive system is already unstable because a less viscous solution $A$ displaces a more viscous solution $B$ (half-plane $R_b > 0$ in **Figure 4**), the reaction modifies the stability properties because, unless $R_c$ and $R_b$ are equal (which is the equivalent of the
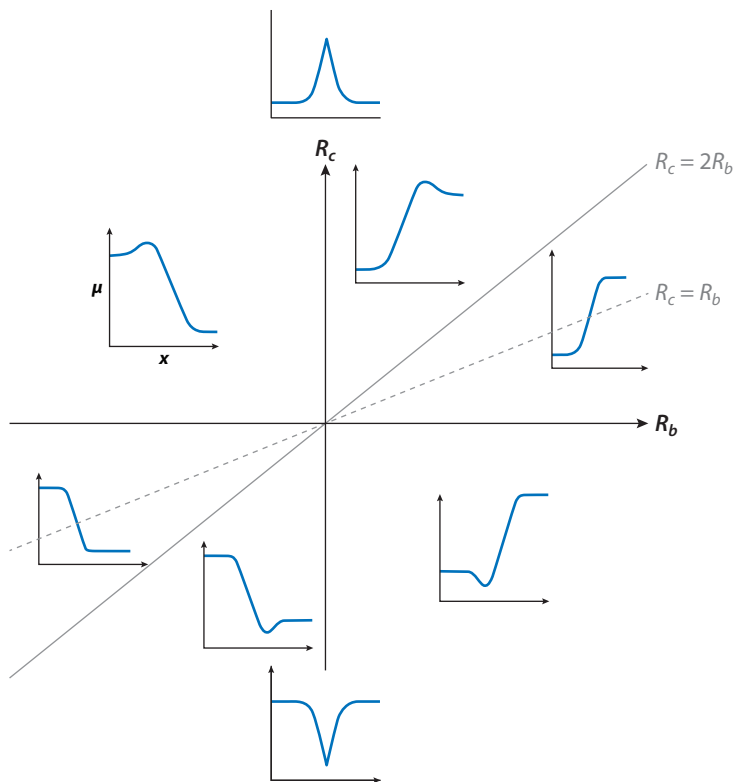


**Figure 4**

Viscosity profiles $\mu(x)$ of a one-dimensional $A + B \rightarrow C$ reaction–diffusion chemical front depending on the relative values of the log mobility ratios $R_b = \ln(\mu_B/\mu_A)$ and $R_c = \ln(\mu_C/\mu_A)$, where $\mu_A$, $\mu_B$, and $\mu_C$ are the viscosities of the reactant solutions $A$ and $B$ and the product $C$, respectively. Figure adapted with permission from Hejazi et al. (2010).

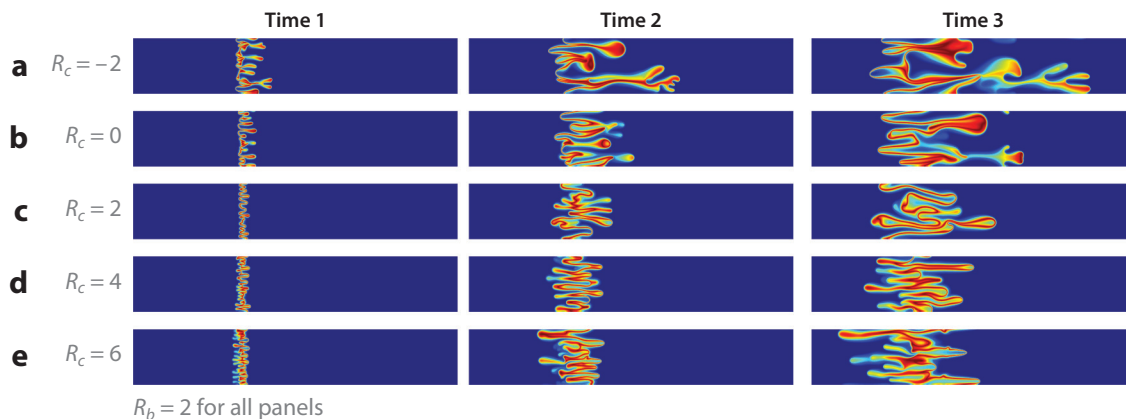|  | Time 1 | Time 2 | Time 3 |
| --- | --- | --- | --- |
| **a** $R_c = -2$ | | | |
| **b** $R_c = 0$ | | | |
| **c** $R_c = 2$ | | | |
| **d** $R_c = 4$ | | | |
| **e** $R_c = 6$ | | | |

$R_b = 2$ for all panels

**Figure 5**

Numerical concentration profiles of product $C$ for a two-dimensional $A + B \rightarrow C$ reaction–diffusion–convection chemical front at three successive times (*left to right*) showing viscous fingering for $R_b = \ln(\mu_B/\mu_A) = 2$, i.e., when the reactant solution of $A$ is injected into the more viscous solution of $B$, and (*a*) $R_c = \ln(\mu_C/\mu_A) = -2$, (*b*) $R_c = 0$, (*c*) $R_c = 2$, (*d*) $R_c = 4$, and (*e*) $R_c = 6$, where $\mu_A$, $\mu_B$, and $\mu_C$ are the viscosities of the solutions of reactants $A$ and $B$ and of the product $C$, respectively.

nonreactive case), the presence of the product $C$ modifies the viscosity profile (Hejazi et al. 2010). LSA predicts that the reactive situations are always more unstable than their nonreactive counterparts for relatively long times because the gradient of viscosity is steepened by the reaction either in the frontal part of the reaction zone, where $C$ pushes $B$ for $R_c < R_b$, or in the rear part of the reaction zone, where $A$ pushes $C$ for $R_c > R_b$. Strikingly, LSA also shows that injecting a more viscous fluid into a less viscous fluid (half-plane $R_b < 0$ in **Figure 4**), a situation classically stable in nonreactive systems, can also induce instabilities when the reaction induces nonmonotonic viscosity profiles (Hejazi et al. 2010). Fingering then develops thanks to the local region where the viscosity increases along the displacement direction. This means that for a nonmonotonic profile with a maximum, fingering develops at the back of the extremum, while in presence of a minimum, fingering is expected in the frontal part of the extremum.

Nonlinear simulations confirm the predictions of LSA in the sense that the reactive cases for $R_b > 0$, some of which are shown in **Figure 5**, are all more unstable than the nonreactive situation, with fingering starting earlier and with a smaller wavelength. These simulations are obtained by numerical integration of Equations 2–6 and 7 in dimensionless streamfunction form with $\kappa$ and $\rho$ constant and variable $R_b$ and $R_c$. Different morphologies of fingers are observed: Fingers become thinner and their centers of mass are more displaced toward the back when $R_c$ is greater than $R_b$ (**Figure 5e**) (Hejazi & Azaiez 2010b, Nagatsu & De Wit 2011). In the case of a maximum in the viscosity profile (zone $R_c > 2R_b > 0$ in **Figure 4**) fingers develop backward in the zone where $A$ pushes the more viscous $C$, while the frontal part, where the more viscous $C$ invades the less viscous $B$, is stable. On the contrary, if $R_c$ is sufficiently lower than $R_b$ such that a minimum of viscosity builds up (zone $R_b > 0$, $R_c < 0$ in **Figure 4**), there is more active forward fingering where less viscous $C$ pushes $B$, while the rear part is stabilized (**Figure 5a**). More efficient coarsening decreases the number of fingers, while tip splitting events are more often observed (Hejazi & Azaiez 2010b, Nagatsu & De Wit 2011). Even if the viscosity ratios of the displaced and displacing solutions in the unfavorable part of the profile are the same, the situation with a minimum of viscosity leads to a faster progression of the fingers at the frontal part with a larger mixing zone than the reverse fingers associated with a maximum of viscosity because the fingers then develop along the flow rather than against it (Mishra et al. 2010a).
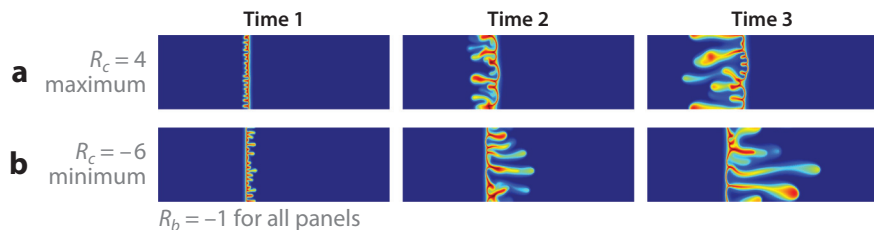
**Time 1**   **Time 2**   **Time 3**

**a** $R_c = 4$ maximum

**b** $R_c = -6$ minimum

$R_b = -1$ for all panels

**Figure 6**

Numerical concentration profiles of product $C$ for a two-dimensional $A + B \rightarrow C$ reaction–diffusion–convection chemical front at three successive times (*left to right*) showing reaction-driven viscous fingering for $R_b = \ln(\mu_B/\mu_A) = -1$, i.e., when the displacing reactant solution of $A$ is more viscous than the invaded solution of $B$. Fingering is triggered by (*a*) a maximum in viscosity for $R_c = \ln(\mu_C/\mu_A) = 4$ or (*b*) a minimum in viscosity for $R_c = -6$, where $\mu_A$, $\mu_B$, and $\mu_C$ are the viscosities of the reactant solutions $A$ and $B$ and the product $C$, respectively.

For $R_b < 0$, the nonreactive case is stable. However, reactions can then trigger fingering when a nonmonotonic viscosity profile builds up. In presence of a minimum in viscosity (zone $R_c < 2R_b < 0$ in **Figure 4**), forward fingering is observed where the less viscous $C$ pushes $B$ (**Figure 6b**). In the case of a maximum in viscosity (zone $R_c > 0, R_b < 0$ in **Figure 4**), the unfavorable viscosity jump is located in the trailing zone where $A$ displaces the more viscous $C$ and reverse fingering is favored (**Figure 6a**). Therefore, this shows that reactions can destabilize an otherwise hydrodynamically stable situation (Riolfo et al. 2012). The case of reversible reactions has also been analyzed, showing that, depending on the viscosities of the reactant and product solutions, reversibility may enhance or attenuate the instability (Alhumade & Azaiez 2013).

Nonlinear simulations have also analyzed the effect of $A + B \rightarrow C$ reactions in the case of a finite-size sample of $B$ displaced in a rectilinear geometry within a fluid $A$. Both interfaces where $A$ pushes $B$ and $B$ pushes $A$ are then present in the same system (Gérard & De Wit 2009, Hejazi & Azaiez 2010a). Such studies also allow analysis of the possible interaction between the two interfaces and to discuss the influence of reactivity on the spreading due to VF of finite-size zones. Even if the reactant solutions have the same viscosity ($R_b = 0$), such fronts can feature different fingering dynamics when the product $C$ is more viscous and the diffusion coefficients or initial concentrations of the two reactants are different (Gérard & De Wit 2009). Indeed, because of the asymmetry of the $C$ concentration profile that different diffusion coefficients or initial concentrations induce (as seen in **Figure 3**), the nonmonotonic viscosity profile is also asymmetric with different unfavorable viscosity gradients depending on whether $A$ or $B$ is the displacing solution. This suggests that the right selection of chemical species with specific differences in concentrations or diffusion coefficients can fine-tune the chemical control of local fingering dynamics. With variable diffusivities, DD effects can also come into play (Mishra et al. 2010b).

The addition of nanocatalysts acting on the reaction rate (Ghesmat et al. 2013; Sabet et al. 2017, 2018; Dastvareh & Azaiez 2019) or the local production of foams (Kahrobaei et al. 2017), which enlarge the range of action, can further control the viscosity profile via extrema to stabilize fingering or, conversely, destabilize an otherwise stable displacement. Interestingly, the geometry also matters, as it has been shown that, in a radial injection, the fact that the local speed decreases with the radius from injection influences the production of $C$ (Brau et al. 2017, Trevelyan & Walker 2018) and thus changes the fingering of finite-size samples (Sharma et al. 2019). In the case where the reactants and the chemical product all have different viscosities, the wealth of possible different dynamics of course increases (Hejazi & Azaiez 2010a).

**6.2.3. Experimental results.** Experiments demonstrating the influence of chemical reactions on the properties of miscible VF are typically conducted in Hele–Shaw cells, which consist of two glass or plexiglass plates separated by a thin gap containing a host solution of a reactant $B$ (Nagatsu 2015). Another reactant $A$ is then injected radially or rectilinearly into the cell at a constant flow rate, and the $A + B \rightarrow C$ reaction then proceeds in the miscible contact zone between them. If the reaction does not change the viscosity in situ, the chemical species are then simply advected by the flow and the concentration pattern depends on the initial concentrations and on the injection flow rate (Nagatsu & Ueda 2001, 2003, 2004; Nagatsu 2015).

Nagatsu et al. (2007) conducted the first experiments on reactive miscible VF where an $A + B \rightarrow C$ type of reaction actively changes the viscosity and hence affects VF. In these experiments, viscous solutions of polymers, the viscosity of which varied with pH, are displaced by less viscous miscible solutions of various reactants. They observed that the fingering pattern is changed by the reaction. If the reaction is very fast, an increase in viscosity induces wider fingers and a suppression of the shielding effect, producing a pattern covering a larger area of the displaced solution. Conversely, a decrease in viscosity leads to thinner fingers with a stronger shielding effect (Nagatsu et al. 2007). This is in good agreement with nonlinear simulations performed for fast reactions (Hejazi & Azaiez 2010b, Nagatsu & De Wit 2011). Interestingly, for slower reactions, the opposite effect is obtained, i.e., wider or thinner fingers respectively for a decrease (Nagatsu et al. 2009) and increase in viscosity (Nagatsu et al. 2011). This can be rationalized by a careful inspection of the relative times of reactions and of advection at the tip or base of the fingers (Nagatsu 2015). In some cases, the polymer used can exhibit non-Newtonian properties. An astonishing growth of fingers in a spiral pattern has then been observed (Nagatsu et al. 2008b). All of these results by Nagatsu et al. showing how the reaction changes the VF pattern were obtained in cases where the less viscous aqueous solution of reactants displaces a more viscous polymeric situation, but where the mobility profile remains monotonic. The nonreactive reference situation is thus already unstable, and reactions change the gradients of viscosities, favoring or slowing down fingering without producing any local extremum in viscosity (zone $2R_b > R_c > 0$ in **Figure 4**).

The case of reactions inducing a nonmonotonic increasing viscosity profile with a maximum (zone $R_c > 2R_b > 0$ in **Figure 4**) has been recently studied in Hele–Shaw cells in the case of a step-growth cross-linking polymerization reaction (Bunton et al. 2017, Stewart et al. 2018). In the absence of reaction, the invading solution is less viscous than the displaced one and VF is obtained. By adding a reaction initiator in variable concentrations in the displacing solution, researchers can tune the amount of the more viscous polymer product in the contact zone. The cross-linked reaction product is more viscous, which results in a nonmonotonic viscosity profile, affecting flow stability. In particular, Bunton et al.'s (2017) experiments recover the numerically predicted fact that fingers extend preferentially at the back of the reaction zone where the less viscous injected reactant displaces the locally produced more viscous product, while the frontal part of the reaction zone is stabilized.

However, the most striking influence of reactions is the ability to destabilize an otherwise hydrodynamically stable displacement, i.e., typically when the displacing solution is more viscous than or of the same viscosity as the displaced solution ($R_b \leq 0$). In the absence of reactions, the interface is stable and no fingering can develop. However, as shown theoretically, extrema in the viscosity profile can destabilize the displacement. Podgorski et al. (2007) experimentally demonstrated for the first time chemically driven VF when the reaction forms a more viscous elastic micellar product following contact between two reactant solutions of the same viscosity (axis $R_c > 0$ for $R_b = 0$ in **Figure 4**). The fingering patterns are different depending on whether $A$ is injected into $B$ or vice versa, which can be related to the asymmetry of the underlying viscosity profiles (Gérard & De Wit 2009) and possible elastic effects. Purely reaction-driven fingering has also
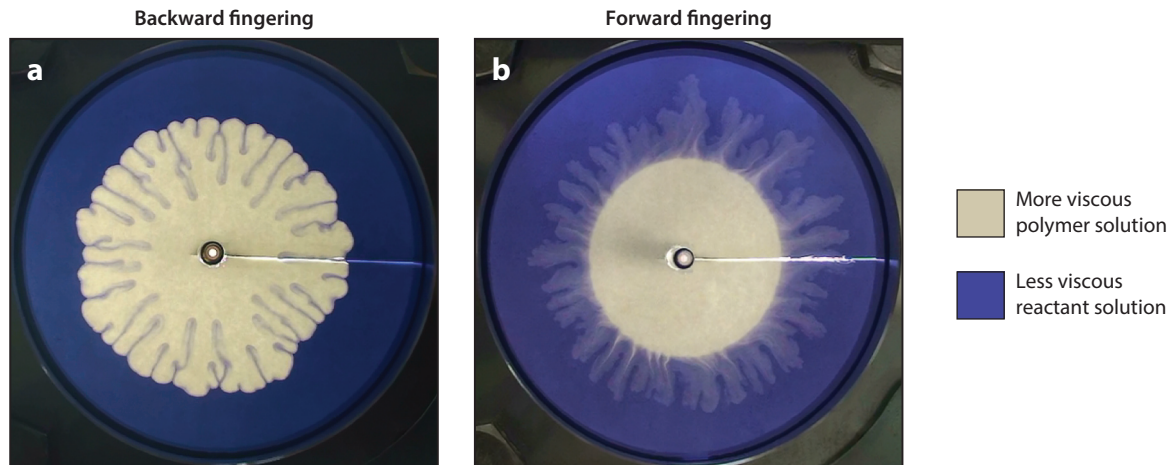
**Backward fingering**

**Forward fingering**



More viscous
polymer solution

Less viscous
reactant solution

**Figure 7**

Experimental evidence of reaction-driven viscous fingering, where a more viscous polymer solution (*white*) displaces a less viscous reactant solution (*blue*) such that the reaction induces (*a*) a local maximum in viscosity, favoring backward fingering, and (*b*) a local minimum in viscosity, inducing forward fingering. Figure adapted with permission from Riolfo et al. (2012).

been obtained when a viscous polymer reaction displaces a less viscous reactant solution (zone $R_b < 0$ in **Figure 4**) and a maximum or minimum in viscosity is produced (Riolfo et al. 2012). As predicted theoretically (Hejazi & Azaiez 2010b, Hejazi et al. 2010, Nagatsu & De Wit 2011), in experiments, fingers are seen to extend backward in case of a maximum and progress ahead of the extremum in case of a minimum (**Figure 7**).

In three-dimensional opaque porous media, reactive fingering has also been analyzed by magnetic resonance. Using the same micelle-producing reaction as Podgorski et al. (2007), Rose & Britton (2013) showed for the first time in three dimensions how the in situ production of the more viscous product can destabilize the displacement of reactant solutions of similar viscosity in a packed bed filled with borosilicate glass beads.

We have reviewed how changes in the mobility profile due to viscosity variations resulting from an $A + B \rightarrow C$ reaction can influence VF and even trigger fingering in otherwise stable nonreactive situations. Recent work has also studied the interplay between fingering and more complex reactions like nonlinear clock reactions (Escala et al. 2019) that can trigger sudden large changes of viscosity (Escala et al. 2017). This is a first step toward using the power of nonlinear oscillating reactions to induce more complex spatiotemporal fingering, including oscillating viscous fingers (Rana & De Wit 2019). We now review instabilities that can result when the mobility profile is related to changes in density.

### 6.3. Buoyancy-Driven Instabilities in Reactive Systems

The density of a solution is a function of its temperature and composition. Of course, some reactions can be exo- or endothermic and thus change both the composition and temperature (Tanoue et al. 2009a,b), but here we neglect heat effects, as they have been shown to be negligible in the experiments described below (Almarcha et al. 2013). When two solutions, each containing a reactive species, are put into contact in the gravity field, local variations in the density due to the reaction can induce convective motion and mixing.

If all three species, $A$, $B$, and $C$, contribute to changes in density, the coupling between the RDC Equations 4–6 for the concentrations and the flow Equation 3 comes from the state equation, $\rho(\mathbf{r}, t) = \rho(a, b, c)$, and the body force of gravity. If the solutions are dilute enough, the density is assumed to vary linearly with concentrations as

$$\rho = \rho_0(1 + \alpha_A a + \alpha_B b + \alpha_C c), \qquad\qquad 9.$$

where $\alpha_i = (\partial \rho / \partial c_i)/\rho_0$ is the solutal expansion coefficient of species $i$, $c_i$ is its concentration, and $\rho_0$ is the density of the solvent. In dimensionless form, the important parameters of the problem are the Rayleigh numbers $R_A$, $R_B$, and $R_C$ of the reactants $A$ and $B$ and the product $C$, respectively, expressing the contribution of each species to the dimensionless density

$$\bar{\rho} = R_A \bar{a} + R_B \bar{b} + R_C \bar{c}, \qquad\qquad 10.$$

where the bar denotes a dimensionless variable. In a porous medium with permeability $\kappa$, the Darcy–Rayleigh numbers can be defined as

$$R_i = \frac{\alpha_i a_0 \kappa l_c}{\nu D_A}, \qquad\qquad 11.$$

where $l_c$ is the characteristic length of the problem and $\nu$ is the kinematic viscosity of the solvent. A large variety of density profiles can then develop, depending on the boundary conditions, concentrations, and diffusion coefficients of the chemical species (Citri et al. 1990).

First, if the initial contact zone between the two solutions is vertical, i.e., parallel to gravity, the front can be influenced by buoyancy-driven convection as soon as the densities of the species differ (Rongy et al. 2008, 2010; Eckert et al. 2012; Tiani et al. 2018). Depending on the later structure of the density profile, one or two convective rolls can deform the front and induce its propagation (Rongy et al. 2008). In particular, one convection roll is obtained for a monotonic density profile as in **Figure 2a,b** when $M = \rho$, while two counter-rotating vortices develop for nonmonotonic profiles as in **Figure 2c,d**. Here again, the mobility profile is the key quantity allowing the prediction of most of the system's behavior.

In the case of a horizontal contact zone between solutions of $A$ and $B$, buoyancy-driven instabilities influenced or triggered by simple $A + B \rightarrow C$ reactions can be divided into three main categories, depending on whether the solutions of $A$ and $B$ are miscible, partially miscible, or immiscible. Below we review each category successively.

## 6.4. Density Fingering of Miscible $A + B \rightarrow C$ Fronts

In the absence of reaction, the stratification of a solution of $A$ above a miscible solution of $B$ induces an RT instability when the upper layer is denser than the lower one. If the initial stratification is initially statically stable (less dense $A$ above denser $B$), a DD instability occurs if $B$ diffuses faster than $A$, while a DLC mode occurs if $A$ diffuses faster than $B$ (Trevelyan et al. 2011).

In reactive systems, we recover the same instabilities when comparing the relative densities and diffusivities of the reactant solutions $A$ and $B$. However, the fact that the product $C$, which has a different density and diffusivity, is generated in situ can change the situation drastically. **Figure 1** compares experimental patterns that have been obtained in Hele–Shaw cells when putting two miscible solutions of different densities into contact along a horizontal plane in the gravity field. As color indicators can play an active role in the dynamics and change the patterns (Almarcha et al. 2010b, Kuster et al. 2011, Mosheva & Shmyrov 2017), **Figure 1** has been obtained using a Schlieren technique tracking changes in the index of refraction. **Figure 1a–c** features mixing

between nonreactive solutions of salt and sugar (Carballido-Landeira et al. 2013, Gopalakrishnan et al. 2018), while **Figure 1d–f** shows the effect of an $A + B \rightarrow C$ neutralization reaction on the stratification between aqueous solutions of a strong acid and of a strong base (Zalts et al. 2008; Tanoue et al. 2009a,b; Almarcha et al. 2010a, 2011; Lemaigre et al. 2013; Bratsun et al. 2015). When the upper solution is denser than the lower one, the initial condition develops an RT instability (**Figure 1a**) with fingers in the nonreactive case extending on average the same distance above and below the initial contact zone. If a reaction takes place, the sinking fingers do not develop because the downward-moving denser $A$ is consumed by the reaction and replaced by a salt of lower density (**Figure 1d**) (Almarcha et al. 2010a, Lemaigre et al. 2013). Similarly, the reaction's local production of the salt $C$ with a different density can break the symmetries of the DD (**Figure 1b,e**) and DLC convective modes (**Figure 1c,f**) (Almarcha et al. 2010a, Lemaigre et al. 2013). In addition, the reactive patterns can feature secondary instabilities in time, for instance, when sufficient production of $C$ triggers the fingered sinking of denser $C$ in the less dense reactant $B$ (Almarcha et al. 2011) or when differential diffusion effects come into play between the zone rich in $C$ and the lower layer of $B$ (Lemaigre et al. 2013). Importantly, even if the reaction is the same (i.e., here, the same acid–base neutralization reaction takes place), the dynamics is extremely sensitive to the nature of the counter-ions, which do not participate in the reaction but have a major role in the density profile and diffusion of the chemicals (Almarcha et al. 2011). Nonideal effects can in some cases influence the dynamics. Indeed, if the solutions are not dilute enough, the diffusion coefficients become a function of the concentrations, which can trigger extrema in nonmonotonic density profiles and induce additional local convection (Bratsun et al. 2015).

Theoretical LSA (Kim 2014), nonlinear simulations (Almarcha et al. 2010a, Lemaigre et al. 2013, Kim 2014), and a classification of all possible density profiles (Almarcha et al. 2011, Lemaigre et al. 2013, Trevelyan et al. 2015) in the parameter space of the problem can explain the experimental observations that chemical reactions can not only trigger instabilities in otherwise stable situations but also break the symmetry of convective structures and instabilities. To understand this, in **Figure 8** we show a variety of possible density profiles around $A + B \rightarrow C$ fronts, depending on the relative values of the Rayleigh numbers and diffusion coefficients of the three species. We see that the density profile can feature up to three extrema in the reaction zone, depending on the values of parameters. These extrema can suppress, trigger, and localize convection and act as efficient controllers of the flows.
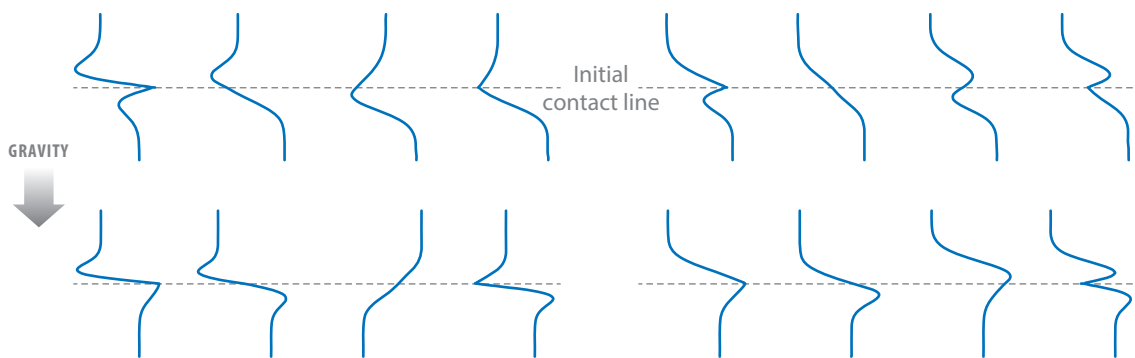


**Figure 8**

A variety of density profiles that can develop around $A + B \rightarrow C$ chemical fronts when all three species have different Rayleigh numbers and diffusion coefficients. The horizontal dashed lines show the position of the initial horizontal contact line between the miscible solutions $A$ and $B$. Figure adapted with permission from Trevelyan et al. (2015).

Hejazi & Azaiez (2012, 2013) have further numerically analyzed the case where the chemical product $C$ has both a different density and a different viscosity than the one of the reactant solutions and a transverse flow is applied parallel to the initial horizontal interface between the reactants. They found that fingers with sharp concentration gradients develop and advance faster downward and that higher chemical production rates are obtained relative to the case without imposed flow.

Recently, chemo-hydrodynamic patterns involving more complex oscillating reactions have been studied as well. In particular, in the $A + B \rightarrow$ oscillator case, separate reactants of an oscillatory reaction are put into contact along a horizontal miscible interface. The oscillations in concentration then develop in the local reaction zone (Escala et al. 2014). As they induce local changes in density, an interplay between localized concentration waves and buoyancy-driven convection produces genuine chemo-hydrodynamic structures that would exist neither in oscillating RD systems nor in pure hydrodynamics. Such studies pave the way toward analyzing patterns that combine the self-organizing structures of chemical and of hydrodynamical systems (Budroni & De Wit 2017).

## 6.5. Influence of $A + B \rightarrow C$ Reactions on Convective Dissolution

The previous section described buoyancy-driven convection around miscible $A + B \rightarrow C$ fronts when convection can extend both above and below the initial contact zone. An important application of similar dynamics but in partially miscible systems is currently attracting a lot of attention: the case of convective dissolution relevant to $CO_2$ sequestration, which aims at reducing atmospheric concentrations of this greenhouse gas (Metz et al. 2005). In this process, $CO_2$ is injected into soils, typically in saline aquifers. After injection, $CO_2$ rises up to the impermeable caprock delimiting the aquifer, and a two-layer stratification of $CO_2$ above the salt water is obtained. Upon dissolution of $CO_2$ in water, a denser boundary layer forms, which can become unstable toward buoyancy-driven convection if thick enough (Riaz et al. 2006, Neufeld et al. 2010, Huppert & Neufeld 2014, Slim 2014, Emami-Meybodi et al. 2015, Thomas et al. 2018). Depending on the chemical composition of the host aquifer, chemical reactions can take place that affect the density profile and hence can affect convection.

The dissolution process results in the stratification of a phase $A$ above $B$ in the host phase with local production of $C$, but the boundary condition is different than the one in the miscible case: The host phase is initially filled only with $B$, and $A$ dissolves into $B$ with a given solubility $a_0$ from an upper fixed interface. Due to the importance for climate issues of quantifying the flux of $CO_2$ that can dissolve in a given host phase, numerous works have focused on analyzing convective dissolution in reactive systems. Here we describe the specificities of this partially miscible case and to what extent reactions can favor convective dissolution.

**6.5.1. Theoretical modeling.** The model equations are again Equations 2–6, and as for the miscible case discussed in Section 6.4, the density is a function of the concentrations $a$, $b$, and $c$ via the state Equation 10. The only differences with the modeling of miscible cases are in the initial conditions ($a = a_0$ at the partially miscible interface and 0 in the bulk, while $b = b_0$ and $c = 0$ everywhere) and the boundary conditions at the interface, where zero velocity and no flux for $B$ and $C$ and $a = a_0$ are applied (Loodts et al. 2016).

These specific initial and boundary conditions induce a downward progression of buoyancy-driven fingers generated at the interface. There is thus a change of symmetry compared to the miscible case. Yet, the analysis of density profiles in the partially miscible case again helps to classify all possible dynamics (Loodts et al. 2016). If all species have the same diffusion coefficients, the
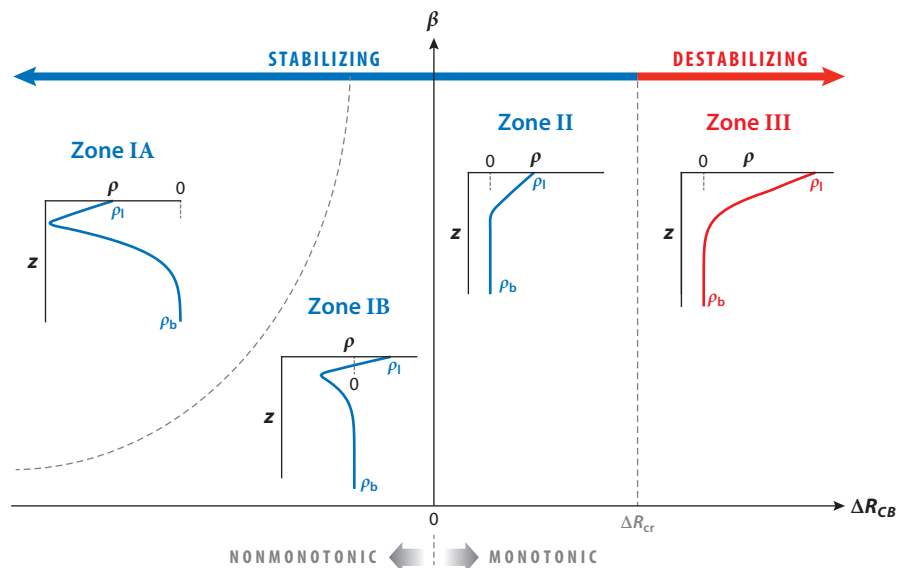
**Figure 9**

Classification of dimensionless density profiles $\rho(z)$ in the parameter space ($\beta = b_0/a_0$, $\Delta R_{CB} = R_C - R_B$), developing when a species $A$ dissolves at $z = 0$ downward into a host phase containing a species $B$ and reacts according to the $A + B \rightarrow C$ scheme to generate the product $C$ (Loodts et al. 2015, 2016; Jotkar et al. 2019). Here $a_0$ and $b_0$ are the solubility of $A$ and the initial concentration of $B$, respectively, while $R_B$ and $R_C$ are the Rayleigh numbers of species $B$ and $C$, respectively. The stability regimes vary depending on whether $\rho(z)$ is nonmonotonic with the density at the interface $\rho_I$ being smaller than the density $\rho_b$ in the bulk (zone IA), nonmonotonic with $\rho_I > \rho_b$ (zone IB), or monotonic (zones II and III). The destabilizing regime (zone III) is obtained when $\Delta R_{CB}$ is larger than a critical value, $\Delta R_{cr}$.

important parameters of the problem are the difference $\Delta R_{CB} = R_C - R_B$ between the Rayleigh numbers of the product $C$ and of the reactant $B$ and the ratio $\beta = b_0/a_0$ between the initial concentration of reactant $B$ and the solubility of $A$ in the host phase.

While simple reactions consuming $A$ out of the solution stabilize convection (Ghesmat et al. 2011; Andres & Cardoso 2011, 2012; Cardoso & Andres 2014; Ward et al. 2014; Kim & Choi 2014; Kim & Kim 2015; Ghoshal et al. 2018), various theoretical works have shown that $A + B \rightarrow C$ reactions can accelerate or decelerate the convective dynamics with respect to the nonreactive case and that the steady-state dissolution flux of species $A$ varies with the difference $\Delta R_{CB}$ (Loodts et al. 2014, 2015, 2017, 2018; Ghoshal et al. 2017; Jotkar et al. 2019). For equal diffusion coefficients and $\Delta R_{CB} > 0$, the density profiles are monotonic. If $C$ is sufficiently denser than $B$, the density at the interface increases, which gives rise to enhanced convective dissolution, a regime that we term "destabilizing" with regard to the nonreactive reference case (**Figure 9**). Conversely, if $C$ is less dense than $B$ ($\Delta R_{CB} < 0$), the density profiles are nonmonotonic. In the upper part of the profile, the density decreases in the direction of gravity, which is prone to trigger convection. However, this zone is followed downward by a stabilizing density barrier that constrains the fingers in a localized zone (Budroni et al. 2014, 2017; Loodts et al. 2018; Jotkar et al. 2019). The resulting nonlinear dynamics can be quite different from the nonreactive case: In the destabilizing case, long sinking fingers form, which regularly merge, while new fingers appear at the boundary (**Figure 10a**). The dynamics caused by chemistry leads to very active renewed convection, as seen on the space–time map of the density along a line just below the interface (**Figure 10b**). In the stabilizing case, the
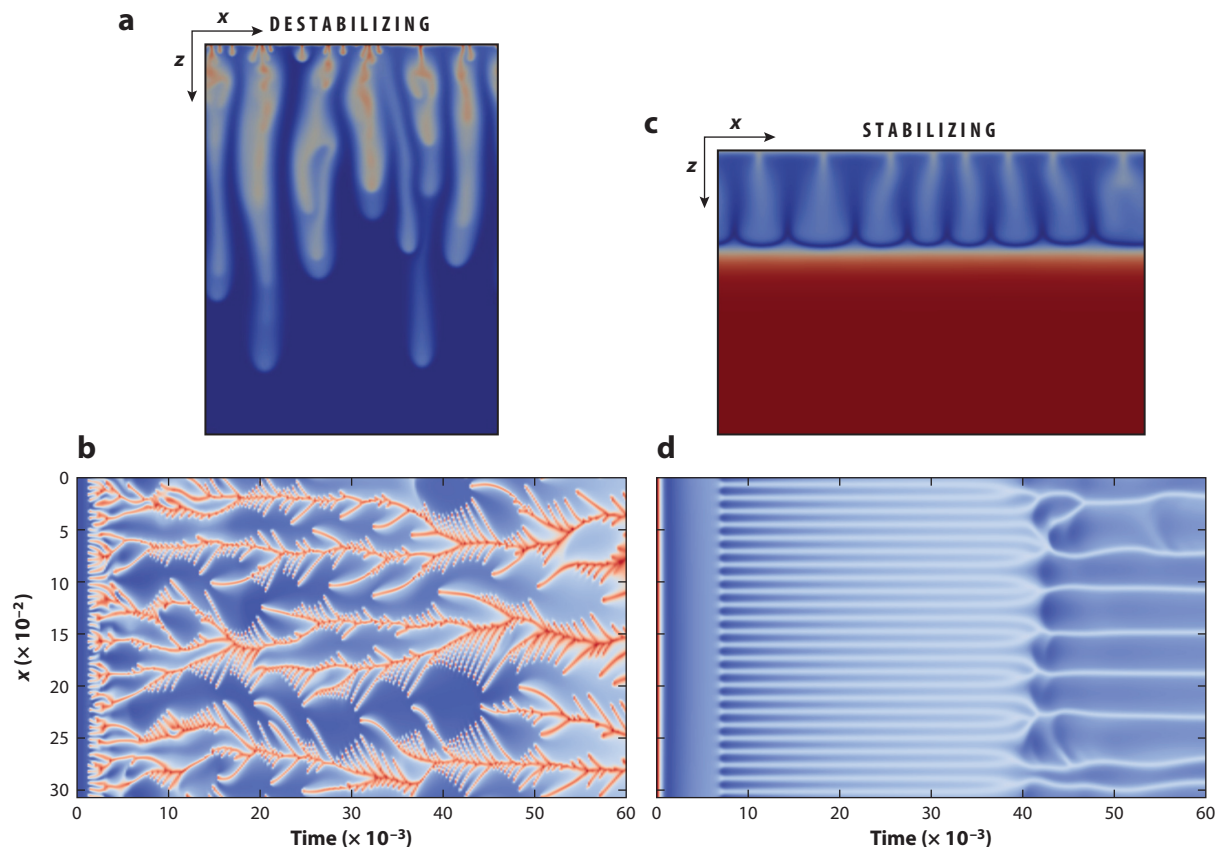
**Figure 10**

Numerical convective dissolution patterns of density on a color scale ranging from blue (minimum) to red (maximum). In the destabilizing case (*a*), fingers sink downward rapidly with very active merging and the formation of new fingers, as seen in the corresponding space–time map (*b*) showing the dynamics along a horizontal line just below the upper interface. In the stabilizing case (*c*), the nonmonotonic density profile with a minimum produces a density barrier, inducing regular fingers with a constant wavelength in time. As seen in the corresponding space–time map (*d*), these fingers rearrange after a while to yield a new frozen pattern but with a larger wavelength (Loodts et al. 2017, Jotkar et al. 2019).

density minimum freezes the fingers above the extremum at a given fixed wavelength (**Figure 10***c*). Only after the reaction front has traveled some distance downward does merging toward a new, larger fixed wavelength occur (**Figure 10***d*). In all reactive cases, the convective flux of $A$ into the host phase is larger than in the nonreactive case (Loodts et al. 2017, Jotkar et al. 2019).

The case of reversible reactions and additional viscosity contrasts has also been analyzed, showing even more complex scenarios (Alhumade & Azaiez 2015). Differential diffusive effects further enlarge the variety of possible dynamics (Kim & Cardoso 2018, Loodts et al. 2018). Similar to VF, buoyancy effects can also be coupled to changes in permeability via reactive dissolution of the porous matrix or precipitation reactions (Ennis-King & Paterson 2007, Ritchie & Pritchard 2011, Hidalgo et al. 2015, Binda et al. 2017). Interestingly, reactions can also destabilize the otherwise stable case of a species dissolving in a host phase and decreasing its density. In that case, the upper layer is less dense, but if reactions come into play, nonmonotonic density profiles can develop, triggering local convection (Bees et al. 2001; Loodts et al. 2015, 2016; Kim & Cardoso 2018).

**6.5.2. Experimental results.** Convective dissolution fingering of $CO_2$ in the absence of any reactions has been experimentally shown in Hele–Shaw cells using a color indicator sensitive to the pH decrease within the fingers as $CO_2$ acidifies the host aqueous phase (Kneafsey & Pruess 2010, 2011). Outeda et al. (2014) studied the temporal evolution of the mixing zone and dispersion curves, as well as the growth rate of the instability for different pressures in $CO_2$ and different color indicator concentrations. They found that, at early times, the growth changes with the concentration of the color indicator and that increasing the pressure destabilizes the system. Using analogous systems, Slim et al. (2013) quantified the nonlinear dynamics, which, as seen in the simulations, features the onset of fingering followed after a while by the merging and regular formation of new fingers. Here again, color indicators can perturb the dynamics (Thomas et al. 2015), which is why Schlieren or interferometric optical techniques tracking index of refraction gradients to visualize convection are preferred techniques. Experiments confirm that the flow is stabilized by first-order reactions where $A$ is consumed and no other species change the density (Cardoso & Andres 2014). Bimolecular $A + B \rightarrow C$ reactions where all species participate in density changes can on the contrary either accelerate or decrease convection (Wylock et al. 2008, 2011, 2014; Budroni et al. 2014, 2017; Loodts et al. 2014; Thomas et al. 2015, 2016; Cherezov & Cardoso 2016). Strikingly, the acceleration is very sensitive to the nature of all ions present in the host phase, which emphasizes the fine-tuning that reactions can have on the control of the density profile (Thomas et al. 2016).

## 6.6. Effect of $A + B \rightarrow C$ Reactions on Buoyancy-Driven Convection in Immiscible Systems

Although not the main focus of this review, we comment here briefly on the immiscible case. Spatiotemporal convective patterns can become quite complex in the case of two immiscible solvents, each containing a reactant, put into contact along a horizontal line. Upon transfer of one reactant from one phase to the other, a wealth of different convective chemo-hydrodynamic patterns can occur in both the upper and lower layers (**Figure 11**) (Eckert & Grahn 1999, Eckert et al. 2004, Asad et al. 2010, Schwarzenberger et al. 2012). The situation is then often complicated by the presence of Marangoni effects due to surface tension gradients (Bratsun & De Wit 2004), and modeling needs to account for RDC equations in both layers (Bratsun & De Wit 2011).
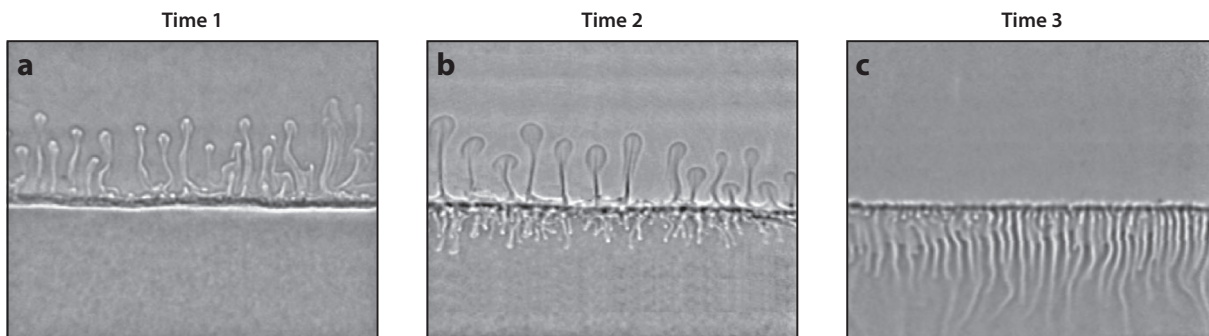
| Time 1 | Time 2 | Time 3 |
|---|---|---|



**Figure 11**

Experimental buoyancy-driven instabilities developing at successive times when an organic upper solvent containing an acid is put into contact with an immiscible lower aqueous solvent containing a base. (*a*) Initially, downward transfer of the acid creates a depletion zone above the interface, inducing upward plumes. (*b*) Next, the acid and base react close to the interface, producing denser sinking fingers of *C* in the lower layer and thermal plumes in the upper layer. (*c*) Later, double-diffusive effects between the various chemicals diffusing at different rates produce regular fingering in the lower layer. Figure adapted from Eckert & Grahn (1999).

# 7. CONCLUSIONS

Chemical reactions can actively influence or even trigger convective motions when two solutions containing separate reactants are put into contact. We have reviewed some of their effects on VF, RT, DD, and convective dissolution instabilities. The key to controlling these various hydrodynamic instabilities by chemical reactions is in the action that reactions can have on the viscosity or density profiles. Specifically, changes in concentration profiles by the local generation of the product of the reaction after consumption of the reactants and the fact that all species can diffuse at different rates can produce local extrema in the mobility profile that can slow down, favor, or generate convection. We have mainly focused on simple $A + B \rightarrow C$ reactions, but more complex reactions giving spatiotemporally complex RD patterns could also be used, increasing the power of chemical control. In this regard, the development of chemo-hydrodynamic pattern selection to predict the properties of hydrodynamic instabilities in active reactive systems should seek for new dynamics existing only thanks to the active coupling between RD and convective modes. The control strategy suggested here relies mainly on controlling the mobility profile that is independent of the flow equation. In that respect, studying the various chemo-hydrodynamic instabilities discussed here in the context of porous media as modeled by Darcy's law, for systems governed by the Stokes or Navier–Stokes equations, is an interesting topic for the future.

## SUMMARY POINTS

1. Chemical reactions can influence and even trigger hydrodynamic instabilities by changing the viscosity, density, or permeability profile.

2. Reactions can break the symmetries of convective instabilities and localize the fluid motions.

3. In viscous fingering, $A + B \rightarrow C$ reactions can enhance or stabilize fingering when a less viscous reactive solution displaces a more viscous one, but they can also trigger an instability when a more viscous solution is the displacing one by generating a local extremum in the viscosity profile.

4. For buoyancy-driven flows, bimolecular reactions change the symmetries of Rayleigh–Taylor, double-diffusive, and convective dissolution patterns and can induce secondary instabilities in time.

5. In convective dissolution, reactions can stabilize or destabilize convection, but in all cases, they increase the dissolution flux toward the host phase.

## FUTURE ISSUES

1. More complex reactions like oscillating reactions could produce pulsatile or patterned convective flows merging the self-organizing power of chemistry and hydrodynamics.

2. A general theory of chemo-hydrodynamic pattern selection should be developed.

3. Generalization of the chemical control of porous media flows to flows described by Stokes or Navier–Stokes equations can be guided by a classification of the dynamics on the basis of the reference mobility profiles.

## DISCLOSURE STATEMENT

The author is not aware of any biases that might be perceived as affecting the objectivity of this review.

## LITERATURE CITED

Alhumade H, Azaiez J. 2013. Stability analysis of reversible reactive flow displacements in porous media. *Chem. Eng. Sci.* 101:46–55

Alhumade H, Azaiez J. 2015. Numerical simulations of gravity driven reversible reactive flows in homogeneous porous media. *Math. Probl. Eng.* 2015:920692

Almarcha C, R'Honi Y, De Decker Y, Trevelyan PMJ, Eckert K, De Wit A. 2011. Convective mixing induced by acid-base reactions. *J. Phys. Chem. B* 104:044501

Almarcha C, Trevelyan PMJ, Grosfils P, De Wit A. 2010a. Chemically driven hydrodynamic instabilities. *Phys. Rev. Lett.* 104:044501

Almarcha C, Trevelyan PMJ, Grosfils P, De Wit A. 2013. Thermal effects on the diffusive layer convection instability of an exothermic acid-base reaction front. *Phys. Rev. E* 88:033009

Almarcha C, Trevelyan PMJ, Riolfo L, Zalts A, El Hasi C, et al. 2010b. Active role of a color indicator in buoyancy-driven instabilities of chemical fronts. *J. Phys. Chem. Lett.* 1:752–57

Andres JTH, Cardoso SSS. 2011. Onset of convection in a porous medium in the presence of a chemical reaction. *Phys. Rev. E* 83:046312

Andres JTH, Cardoso SSS. 2012. Convection and reaction in a diffusive boundary layer in a porous medium: nonlinear dynamics. *Chaos* 22:037113

Asad A, Yang YH, Chai C, Wu J. 2010. Hydrodynamic instabilities driven by acid-base neutralization reaction in immiscible system. *Chin. J. Chem. Phys.* 23:513–20

Bees MA, Pons AJ, Sørensen PG, Sagués F. 2001. Chemoconvection: a chemically driven hydrodynamic instability. *J. Chem. Phys.* 114:1932

Binda L, El Hasi C, Zalts A, D'Onofrio A. 2017. Experimental analysis of density fingering instability modified by precipitation. *Chaos* 27:053111

Bratsun D, De Wit A. 2004. On Marangoni convective patterns driven by an exothermic chemical reaction in two-layer systems. *Phys. Fluids* 16:1082–96

Bratsun D, De Wit A. 2011. Buoyancy-driven pattern formation in reactive immiscible two-layer systems. *Chem. Eng. Sci.* 66:5723–34

Bratsun D, Kostarev K, Mizev A, Mosheva E. 2015. Concentration-dependent diffusion instability in reactive miscible fluids. *Phys. Rev. E* 92:011003(R)

Brau F, Schuszter G, De Wit A. 2017. Flow control of $A + B \to C$ fronts by radial injection. *Phys. Rev. Lett.* 118:134101

Broyles B, Shalliker R, Cherrak D, Guiochon G. 1998. Visualization of viscous fingering in chromatographic columns. *J. Chromatog. A* 822:173–87

Budroni MA, De Wit A. 2017. Dissipative structures: from reaction-diffusion to chemo-hydrodynamic patterns. *Chaos* 27:104617

Budroni MA, Riolfo LA, Lemaigre L, Rossi F, Rustici M, De Wit A. 2014. Chemical control of hydrodynamic instabilities in partially miscible two-layer systems. *J. Phys. Chem. Lett.* 5:875–81

Budroni MA, Thomas C, De Wit A. 2017. Chemical control of dissolution-driven convection in partially miscible systems: nonlinear simulations and experiments. *Phys. Chem. Chem. Phys.* 19:7936–46

Bunton P, Tullier M, Meiburg E, Pojman J. 2017. The effect of a crosslinking chemical reaction on pattern formation in viscous fingering of miscible fluids in a Hele–Shaw cell. *Chaos* 27:104614

Carballido-Landeira J, Trevelyan P, Almarcha C, De Wit A. 2013. Mixed-mode instability of a miscible interface due to coupling between Rayleigh-Taylor and double-diffusive convective modes. *Phys. Fluids* 25:024107

Cardoso SSS, Andres JTH. 2014. Geochemistry of silicate-rich rocks can curtail spreading of carbon dioxide in subsurface aquifers. *Nat. Commun.* 5:5743

Chadam J, Hoff D, Merino E, Ortoleva P, Sen A. 1986. Reactive infiltration instabilities. *IMA J. Appl. Math.* 36:207–21

Cherezov I, Cardoso SSS. 2016. Acceleration of convective dissolution by chemical reaction in a Hele-Shaw cell. *Phys. Chem. Chem. Phys.* 18:23727–36

Citri O, Kagan M, Kosloff R, Avnir D. 1990. Evolution of chemically induced unstable density gradients near horizontal reactive interfaces. *Langmuir* 6:559–64

Daccord G, Lenormand R. 1987. Fractal patterns from chemical dissolution. *Nature* 325:41–43

Dastvareh B, Azaiez J. 2019. Instabilities of nonisothermal nanocatalytic reactive flows in porous media. *Phys. Rev. Fluids* 4:034003

De Wit A. 2016. Chemo-hydrodynamic patterns in porous media. *Philos. Trans. R. Soc. A* 374:20150419

De Wit A, Bertho Y, Martin M. 2005. Viscous fingering of miscible slices. *Phys. Fluids* 17:054114

De Wit A, Eckert K, Kalliadasis S. 2012. Introduction to the focus issue: chemo-hydrodynamic patterns and instabilities. *Chaos* 22:037101

De Wit A, Homsy GM. 1999a. Nonlinear interactions of chemical reactions and viscous fingering in porous media. *Phys. Fluids* 11:949–51

De Wit A, Homsy GM. 1999b. Viscous fingering in reaction-diffusion systems. *J. Chem. Phys.* 110:8663–75

Dickson ML, Norton TT, Fernandez EJ. 1997. Chemical imaging of multicomponent viscous fingering in chromatography. *AIChE J.* 43:409–18

Eckert K, Acker M, Shi Y. 2004. Chemical pattern formation driven be a neutralization reaction. I. Mechanism and basic features. *Phys. Fluids* 16:385–99

Eckert K, Acker M, Tadmouri R, Pimienta V. 2012. Chemo-Marangoni convection driven by an interfacial reaction: pattern formation and kinetics. *Chaos* 22:037112

Eckert K, Grahn A. 1999. Plume and finger regimes driven by an exothermic interfacial reaction. *Phys. Rev. Lett.* 82:4436

Emami-Meybodi H, Hassanzadeh H, Green CP, Ennis-King J. 2015. Convective dissolution of $CO_2$ in saline aquifers: progress in modeling and experiments. *Int. J. Greenh. Gas Control* 40:238–66

Ennis-King J, Paterson L. 2007. Coupling of geochemical reactions and convective mixing in the long-term geological storage of carbon dioxide. *Int. J. Greenh. Gas Control* 1:86–93

Escala DM, Budroni MA, Carballido-Landeira J, De Wit A, Muñuzuri AP. 2014. Self-organized traveling chemo-hydrodynamic fingers triggered by a chemical oscillator. *J. Phys. Chem. Lett.* 5:413–18

Escala DM, De Wit A, Carballido-Landeira J, Muñuzuri AP. 2019. Viscous fingering induced by a pH-sensitive clock reaction. *Langmuir* 35:4182–88

Escala DM, Muñuzuri AP, De Wit A, Carballido-Landeira J. 2017. Temporal viscosity modulations driven by a pH sensitive polymer coupled to a pH-changing chemical reaction. *Phys. Chem. Chem. Phys.* 19:11914–19

Fernandez J, Homsy GM. 2003. Viscous fingering with chemical reaction: effect of in-situ production of surfactants. *J. Fluid Mech.* 480:267–81

Fernandez J, Kurowski P, Petitjeans P, Meiburg E. 2002. Density-driven unstable flows of miscible fluids in a Hele-Shaw cell. *J. Fluid Mech.* 451:239–60

Gálfi L, Rácz Z. 1988. Properties of the reaction front in an $A + B \rightarrow C$ type reaction-diffusion process. *Phys. Rev. A* 38:3151–54

Gérard T, De Wit A. 2009. Miscible viscous fingering induced by a simple $A + B \rightarrow C$ chemical reaction. *Phys. Rev. E* 79:016308

Ghesmat K, Azaiez J. 2009. Miscible displacements of reactive and anisotropic dispersive flows in porous media. *Transp. Porous Media* 77:489–506

Ghesmat K, Hassanzadeh H, Abedi J. 2011. The impact of geochemistry on convective mixing in a gravitationally unstable diffusive boundary layer in porous media: $CO_2$ storage in saline aquifers. *J. Fluid Mech.* 673:480–512

Ghesmat K, Hassanzadeh H, Abedi J, Chen Z. 2013. Frontal stability of reactive nanoparticle transport during in situ catalytic upgrading of heavy oil. *Fuel* 107:525–38

Ghoshal P, Kim MC, Cardoso SSS. 2017. Reactive-convective dissolution in a porous medium: the storage of carbon dioxide in saline aquifers. *Phys. Chem. Chem. Phys.* 19:644–55

Ghoshal P, Kim MC, Cardoso SSS. 2018. Onset of convection in the presence of a precipitation reaction in a porous medium: a comparison of linear stability and numerical approaches. *Fluids* 3:1

Gopalakrishnan SS, Carballido-Landeira J, Knaepen B, De Wit A. 2018. Control of Rayleigh-Taylor instability onset time and convective velocity by differential diffusion effects. *Phys. Rev. E* 98:011101(R)

Guiochon G, Felinger A, Shirazi DG, Katti AM. 2006. *Fundamentals of Preparative and Nonlinear Chromatography*. New York: Academic

Haudin F, Cartwright JHE, Brau F, De Wit A. 2014. Spiral precipitation patterns in confined chemical gardens. *PNAS* 111:17363–67

Haudin F, De Wit A. 2015. Patterns due to an interplay between viscous and precipitation-driven fingering. *Phys. Fluids* 27:113101

Hejazi SH, Azaiez J. 2010a. Hydrodynamic instability in the transport of miscible reactive slices through porous media. *Phys. Rev. E* 81:056321

Hejazi SH, Azaiez J. 2010b. Non-linear interactions of dynamic interfaces in porous media. *Chem. Eng. Sci.* 65:938

Hejazi SH, Azaiez J. 2012. Stability of reactive interfaces in saturated porous media under gravity in the presence of transverse flows. *J. Fluid Mech.* 695:439–66

Hejazi SH, Azaiez J. 2013. Nonlinear simulation of transverse flow interactions with chemically driven convective mixing in porous media. *Water Resour. Res.* 49:4607–18

Hejazi SH, Trevelyan PMJ, Azaiez J, De Wit A. 2010. Viscous fingering of a miscible reactive $A + B \rightarrow C$ interface: a linear stability analysis. *J. Fluid Mech.* 652:501–28

Hidalgo JJ, Dentz M, Cabeza Y, Carrera J. 2015. Dissolution patterns and mixing dynamics in unstable reactive flow. *Geophys. Res. Lett.* 42:6357–64

Hill S. 1952. Channelling in packed columns. *Chem. Eng. Sci.* 1:247–53

Homsy GM. 1987. Viscous fingering in porous media. *Annu. Rev. Fluid Mech.* 19:271–311

Hornof V, Baig FU. 1995. Influence of interfacial reaction and mobility ratio on the displacement of oil in a Hele-Shaw cell. *Exp. Fluids* 18:448–53

Hota T, Pramanik S, Mishra M. 2015. Onset of fingering instability in a finite slice of adsorbed solute. *Phys. Rev. E* 92:023013

Huppert HE, Neufeld JA. 2014. The fluid mechanics of carbon dioxide sequestration. *Annu. Rev. Fluid Mech.* 46:255–72

Jahoda M, Hornof V. 2000. Concentration profiles of reactant in a viscous finger formed during the interfacially reactive immiscible displacements in porous media. *Powder Technol.* 110:253–57

Jiang Z, Ebner C. 1990. Simulation study of reaction fronts. *Phys. Rev. A* 42:7483–86

Jotkar M, De Wit A, Rongy L. 2019. Enhanced convective dissolution due to an $A + B \rightarrow C$ reaction: control of the non-linear dynamics via solutal density contributions. *Phys. Chem. Chem. Phys.* 21:6432–42

Kahrobaei S, Vincent-Bonnieu S, Farajzadeh R. 2017. Experimental study of hysteresis behavior of foam generation in porous media. *Sci. Rep.* 7:8986

Kim M. 2014. Effect of the irreversible $A + B \rightarrow C$ reaction on the onset and the growth of the buoyancy-driven instability in a porous medium. *Chem. Eng. Sci.* 112:56–71

Kim MC, Cardoso SSS. 2018. Diffusivity ratio effect on the onset of the buoyancy-driven instability of an $A + B \rightarrow C$ chemical reaction system in a Hele-Shaw cell: asymptotic and linear stability analyses. *Phys. Fluids* 30:094102

Kim MC, Choi CK. 2014. Effect of first-order chemical reaction on gravitational instability in a porous medium. *Phys. Rev. E* 90:053016

Kim MC, Kim YH. 2015. The effect of chemical reaction on the onset of gravitational instabilities in a fluid saturated within a vertical Hele-Shaw cell: theoretical and numerical studies. *Chem. Eng. Sci.* 134:632–47

Kneafsey T, Pruess K. 2010. Laboratory flow experiments for visualizing carbon dioxide-induced, density-driven brine convection. *Transp. Porous Media* 82:123–39

Kneafsey T, Pruess K. 2011. Laboratory experiments and numerical simulation studies of convectively enhanced carbon dioxide dissolution. *Energy Procedia* 4:5114–21

Kuster S, Riolfo L, Zalts A, El Hasi C, Almarcha C, et al. 2011. Differential diffusion effects on buoyancy-driven instabilities of acid-base fronts: the case of a color indicator. *Phys. Chem. Chem. Phys.* 13:17295–303

Lemaigre L, Budroni MA, Riolfo LA, Grosfils P, De Wit A. 2013. Asymmetric Rayleigh-Taylor and double-diffusive fingers in reactive systems. *Phys. Fluids* 25:014103

Loodts V, Knaepen B, Rongy L, De Wit A. 2017. Enhanced steady-state dissolution flux in reactive convective dissolution. *Phys. Chem. Chem. Phys.* 19:18565–79

Loodts V, Rongy L, De Wit A. 2014. Impact of pressure, salt concentration, and temperature on the convective dissolution of carbon dioxide in aqueous solutions. *Chaos* 24:043120

Loodts V, Rongy L, De Wit A. 2015. Chemical control of dissolution-driven convection in partially miscible systems: theoretical classification. *Phys. Chem. Chem. Phys.* 17:29814–23

Loodts V, Saghou H, Knaepen B, Rongy L, De Wit A. 2018. Differential diffusivity effects in reactive convective dissolution. *Fluids* 3:83

Loodts V, Trevelyan PMJ, Rongy L, De Wit A. 2016. Density profiles around $A + B \rightarrow C$ reaction-diffusion fronts in partially miscible systems: a general classification. *Phys. Rev. E* 94:043115

Manickam O, Homsy G. 1995. Fingering instabilities in vertical miscible displacement flows in porous media. *J. Fluid Mech.* 288:75–102

Meiburg E, Kneller B. 2010. Turbidity currents and their deposits. *Annu. Rev. Fluid Mech.* 42:135–56

Metz B, Davidson O, de Conninck H, Loos M, Meyer L, eds. 2005. *Carbon Dioxide Capture and Storage*. Cambridge, UK: Cambridge Univ. Press

Mishra M, Martin M, De Wit A. 2007. Miscible viscous fingering with linear adsorption on the porous matrix. *Phys. Fluids* 19:073101

Mishra M, Martin M, De Wit A. 2010a. Influence of miscible viscous fingering with negative log-mobility ratio on spreading of adsorbed analytes. *Chem. Eng. Sci.* 65:2392–98

Mishra M, Trevelyan P, Almarcha C, De Wit A. 2010b. Influence of double diffusive effects on miscible viscous fingering. *Phys. Rev. Lett.* 105:204501

Mosheva E, Shmyrov A. 2017. Effect of the universal acid-base indicator on the formation of the concentration-dependent diffusion instability. *IOP Conf. Ser. Mater. Sci. Eng.* 208:012029

Nagatsu Y. 2015. Viscous fingering phenomena with chemical reactions. *Curr. Phys. Chem.* 5:52–63

Nagatsu Y, Bae SK, Kato Y, Tada Y. 2008a. Miscible viscous fingering with a chemical reaction involving precipitation. *Phys. Rev. E* 77:067302

Nagatsu Y, De Wit A. 2011. Viscous fingering of a miscible reactive $A + B \rightarrow C$ interface for an infinitely fast chemical reaction: nonlinear simulations. *Phys. Fluids* 23:043103

Nagatsu Y, Hayashi A, Ban M, Kato Y, Tada Y. 2008b. Spiral pattern in a radial displacement involving a reaction-producing gel. *Phys. Rev. E* 78:026307

Nagatsu Y, Ishii Y, Tada Y, De Wit A. 2014. Hydrodynamic fingering instability induced by a precipitation reaction. *Phys. Rev. Lett.* 113:024502

Nagatsu Y, Kondo Y, Kato Y, Tada Y. 2009. Effects of moderate Damköhler number on miscible viscous fingering involving viscosity decrease due to a chemical reaction. *J. Fluid Mech.* 625:97–124

Nagatsu Y, Kondo Y, Kato Y, Tada Y. 2011. Miscible viscous fingering involving viscosity increase by a chemical reaction with moderate Damköhler number. *Phys. Fluids* 23:014109

Nagatsu Y, Matsuda K, Kato Y, Tada Y. 2007. Experimental study on miscible viscous fingering involving viscosity changes induced by variations in chemical species concentrations due to chemical reactions. *J. Fluid Mech.* 571:475–93

Nagatsu Y, Ueda T. 2001. Effects of reactant concentrations on reactive miscible viscous fingering. *AIChE J.* 47:1711–20

Nagatsu Y, Ueda T. 2003. Effects of finger-growth velocity on reactive miscible viscous fingering. *AIChE J.* 49:789–92

Nagatsu Y, Ueda T. 2004. Analytical study on effects of finger-growth velocity on reaction characteristics of reactive miscible viscous fingering by using a convection–diffusion–reaction model. *Chem. Eng. Sci.* 59:3817–26

Nasr-El-Din H, Khulbe K, Hornof V, Neale G. 1990. Effects of interfacial reaction on the radial displacement of oil by alkaline solutions. *Rev. Inst. Fr. Pétr.* 45:231–44

Neufeld JA, Hesse M, Riaz A, Hallworth MA, Tchelepi HA, Huppert HE. 2010. Convective dissolution of carbon dioxide in saline aquifers. *Geophys. Res. Lett.* 37:L22404

Niroobakhsh Z, Litman M, Belmonte A. 2017. Flow instabilities due to the interfacial formation of surfactant-fatty acid material in a Hele-Shaw cell. *Phys. Rev. E* 96:053102

Outeda R, El Hasi C, D'Onofrio A, Zalts A. 2014. An experimental study of linear and nonlinear regimes of density-driven instabilities induced by $CO_2$ dissolution in water. *Chaos* 24:013135

Podgorski T, Sostarecz MC, Zorman S, Belmonte A. 2007. Fingering instabilities of a reactive micellar interface. *Phys. Rev. E* 79:016202

Radko T. 2013. *Double-Diffusive Convection*. Cambridge, UK: Cambridge Univ. Press

Rana C, De Wit A. 2019. Reaction-driven oscillating viscous fingering. *Chaos* 29:043115

Rana C, De Wit A, Martin M, Mishra M. 2014. Combined influences of viscous fingering and solvent effect on the distribution of adsorbed solutes in porous media. *RSC Adv.* 4:34369–81

Rana C, Mishra M, De Wit A. 2018. Effect of anti-Langmuir adsorption on spreading in porous media. *Europhys. Lett.* 124:64003

Riaz A, Hesse M, Tchelepi HA, Orr FM Jr. 2006. Onset of convection in a gravitationally unstable diffusive boundary layer in porous media. *J. Fluid Mech.* 548:87–111

Riolfo LA, Nagatsu Y, Iwata S, Maes R, Trevelyan PMJ, De Wit A. 2012. Experimental evidence of reaction-driven miscible viscous fingering. *Phys. Rev. E* 85:015304(R)

Ritchie L, Pritchard D. 2011. Natural convection and the evolution of a reactive porous medium. *J. Fluid Mech.* 673:286–317

Rongy L, Trevelyan P, De Wit A. 2008. Dynamics of $A + B \rightarrow C$ reaction fronts in the presence of buoyancy-driven convection. *Phys. Rev. Lett.* 101:084503

Rongy L, Trevelyan P, De Wit A. 2010. Influence of buoyancy-driven convection on the dynamics of $A + B \rightarrow C$ reaction fronts in horizontal solution layers. *Chem. Eng. Sci.* 65:2382–91

Rose H, Britton M. 2013. Magnetic resonance imaging of reaction-driven viscous fingering in a packed bed. *Microporous Mesoporous Mater.* 178:64–68

Rousseaux G, De Wit A, Martin M. 2007. Viscous fingering in packed chromatographic columns: linear stability analysis. *J. Chromatogr. A* 1149:254–73

Rousseaux G, Martin M, De Wit A. 2011. Viscous fingering in packed chromatographic columns: non-linear dynamics. *J. Chromatogr. A* 1218:8353–61

Sabet N, Hassanzadeh H, Abedi J. 2017. Control of viscous fingering by nanoparticles. *Phys. Rev. E* 96:063114

Sabet N, Raad S, Hassanzadeh H, Abedi J. 2018. Dynamics of miscible nanocatalytic reactive flows in porous media. *Phys. Rev. Appl.* 10:054033

Saffman PG, Taylor GI. 1958. The penetration of a fluid into a porous medium or Hele-Shaw cell containing a more viscous liquid. *Proc. R. Soc. Lond. A* 245:312–29

Schuszter G, Brau F, De Wit A. 2014. Calcium carbonate mineralization in a confined geometry. *Environ. Sci. Technol. Lett.* 3:156–59

Schwarzenberger K, Eckert K, Odenbach S. 2012. Relaxation oscillations between Marangoni cells and double diffusive fingers in a reactive liquid–liquid system. *Chem. Eng. Sci.* 68:530–40

Sharma V, Pramanik S, Chen CY, Mishra M. 2019. A numerical study on reaction-induced radial fingering instability. *J. Fluid Mech.* 862:624–38

Slim AC. 2014. Solutal-convection regimes in a two-dimensional porous medium. *J. Fluid Mech.* 741:461–91

Slim AC, Bandi MM, Miller JC, Mahadevan L. 2013. Dissolution-driven convection in a Hele–Shaw cell. *Phys. Fluids* 25:024101

Stewart S, Marin D, Tullier M, Pojman J, Meiburg E, Bunton P. 2018. Stabilization of miscible viscous fingering by a step growth polymerization reaction. *Exp. Fluids* 59:114

Swernath S, Pushpavanam S. 2007. Viscous fingering in a horizontal flow through a porous medium induced by chemical reactions under isothermal and adiabatic conditions. *J. Chem. Phys.* 127:204701

Swernath S, Pushpavanam S. 2008. Instability of a vertical chemical front: effect of viscosity and density varying with concentration. *Phys. Fluids* 20:012101

Szymczak P, Ladd AJC. 2014. Reactive-infiltration instabilities in rocks. Part 2. Dissolution of a porous matrix. *J. Fluid Mech.* 738:591–630

Tanoue K, Ikemoto H, Yoshitomi M, Nishimura T. 2009a. Instabilized heat and mass transfer in exothermic chemically reacting flows. *Therm. Sci. Eng.* 17:121–29

Tanoue K, Yoshitomi M, Nishimura T. 2009b. Heat transfer under buoyancy-induced flow at the chemical reaction front using thermochromic liquid crystal sheet. *J. Chem. Eng. Jpn.* 42:255–58

Thomas C, Dehaeck S, De Wit A. 2018. Convective dissolution of $CO_2$ in water and salt solutions. *Int. J. Greenh. Gas Control* 72:105–16

Thomas C, Lemaigre L, Zalts A, D'Onofrio A, De Wit A. 2015. Experimental study of $CO_2$ convective dissolution: the effect of color indicators. *Int. J. Greenh. Gas Control* 42:525–33

Thomas C, Loodts V, Rongy L, De Wit A. 2016. Convective dissolution of $CO_2$ in reactive alkaline solutions: active role of spectator ions. *Int. J. Greenh. Gas Control* 53:230–42

Tiani R, De Wit A, Rongy L. 2018. Surface tension and buoyancy-driven flows across horizontally propagating chemical fronts. *Adv. Colloid Interface Sci.* 225:76–83

Trevelyan PMJ, Almarcha C, De Wit A. 2011. Buoyancy-driven instabilities of miscible two-layer stratifications in porous media and Hele-Shaw cells. *J. Fluid Mech.* 670:38–65

Trevelyan PMJ, Almarcha C, De Wit A. 2015. Buoyancy-driven instabilities around miscible $A + B \rightarrow C$ reaction fronts: a general classification. *Phys. Rev. E* 91:023001

Trevelyan PMJ, Walker A. 2018. Asymptotic properties of radial $A + B \rightarrow C$ reaction fronts. *Phys. Rev. E* 98:032118

Tsuzuki R, Ban T, Fujimura M, Nagatsu Y. 2019. Dual role of surfactant-producing reaction in immiscible viscous fingering evolution. *Phys. Fluids* 31:022102

Turner J. 1979. *Buoyancy Effects in Fluids*. Cambridge, UK: Cambridge Univ. Press

Villermaux E. 2019. Mixing versus stirring. *Annu. Rev. Fluid Mech.* 51:245–73

Ward TJ, Cliffe KA, Jensen OE, Power H. 2014. Dissolution-driven porous-medium convection in the presence of chemical reaction. *J. Fluid Mech.* 747:316–49

White A, Ward T. 2012. $CO_2$ sequestration in a radial Hele-Shaw cell via an interfacial chemical reaction. *Chaos* 22:037114

Wooding RA. 1969. Growth of fingers at an unstable diffusing interface in a porous medium or Hele-Shaw cell. *J. Fluid Mech.* 39:477–95

Wylock C, Dehaeck S, Cartage T, Colinet P, Haut B. 2011. Experimental study of gas–liquid mass transfer coupled with chemical reactions by digital holographic interferometry. *Chem. Eng. Sci.* 66:3400–12

Wylock C, Dehaeck S, Rednikov A, Colinet P. 2008. Chemo-hydrodynamical instability created by $CO_2$ absorption in an aqueous solution of $NaHCO_3$ and $Na_2CO_3$. *Microgravity Sci. Technol.* 20:171

Wylock C, Rednikov A, Haut B, Colinet P. 2014. Nonmonotonic Raleigh-Taylor instabilities driven by gas–liquid $CO_2$ chemisorption. *J. Phys. Chem. B* 118:11323–29

Zalts A, El Hasi C, Rubio D, Urena A, D'Onofrio A. 2008. Pattern formation driven by an acid-base neutralization reaction in aqueous media in a gravitational field. *Phys. Rev. E* 77:015304(R)

# Contents

## Indexes

## Errata

An online log of corrections to *Annual Review of Fluid Mechanics* articles may be found
at http://www.annualreviews.org/errata/fluid